

Comparing slab and height-resolving models of the tropical cyclone boundary layer

Jeffrey D. Kepert *

Centre for Australian Weather and Climate Research

A partnership between the Australian Bureau of Meteorology and CSIRO

9th International Conference on Southern Hemisphere Meteorology and Oceanography, Feb 9 – 13, 2009

1. Introduction

Understanding the dynamics of the tropical cyclone boundary layer (TCBL) is important, since

1. the boundary layer winds determine much of the impact of the cyclone upon humanity, either directly or through their influence on the sea, and
2. the latent heat release in the eyewall and spiral rain bands that fuels the storm depends on the supply of warm moist energy-rich air from the boundary layer into the base of these clouds.

Understanding of the TCBL is thus critical to forecasting and to risk assessment, and is a key factor that impacts the intensity and potential intensity of tropical cyclones.

A range of simplified models have been developed to improve understanding of the tropical cyclone boundary layer. Many of these models seek to diagnose the boundary layer flow in response to some applied forcing pressure field representative of that part of the cyclone above the boundary layer, and differ chiefly in the assumptions and simplifications made in the search for a solution. Common simplifications are the use of depth-averaged equations and the assumption of axisymmetry, leading to a convenient categorization of these models:

- *Column models*: The one-dimensional single-column model of Deardorff (1972) was extended to the TCBL by Moss and Rosenthal (1975) and further refined by Powell (1980) and Powell

et al. (1996) and used for estimating surface winds from aircraft data.

- *Depth-averaged (also known as slab) axisymmetric*: Smith (2003), Smith and Vogl (2008). A simplified depth-averaged boundary layer model is an essential component of Emanuel's potential intensity theory (Emanuel 1988, 1995; Bister and Emanuel 1998).
- *Depth-averaged, non-symmetric*: Shapiro (1983), Vickery *et al.* (2000)
- *Prescribed vertical structure, axisymmetric*: Smith (1968), Leslie and Smith (1970), Bode and Smith (1975).
- *Height-resolving, axisymmetric*: Rosenthal (1962), Eliassen and Lystad (1977), Montgomery *et al.* (2001), Kuo (1971, 1982)
- *Height-resolving, non-symmetric*: Kepert (2001), Kepert and Wang (2001)

These models have had considerable success in predicting and explaining observed features of the tropical cyclone boundary layer. For example, the increase in the ratio of the surface wind speed to that at flight level found by Franklin *et al.* (2003) in their analysis of dropsonde data was predicted by Kepert (2001) and Kepert and Wang (2001). Similarly, those latter authors' prediction of supergradient flow in the upper boundary layer in the tropical cyclone inner core has been subsequently confirmed by observational analyses (Kepert 2006a,b; Bell and Montgomery 2008; Schwendike and Kepert 2008).

The above classification of models, while useful, does obscure some important differences between models in the same class.

*Centre for Australian Weather and Climate Research, Bureau of Meteorology, 700 Collins St, Melbourne Vic 3000. Email: J.Kepert@bom.gov.au

These differences have recently been analysed in the context of axisymmetric slab models by Smith *et al.* (2008) and Smith and Montgomery (2008), who have shown that various further linearisations or balance assumptions in depth-averaged models can have significant effects on the solutions obtained.

With the recent advent of 3-dimensional simplified models, is there still a need for the simpler models, particularly the axisymmetric depth-averaged models? We believe that the answer to this question is, with some qualifications, yes. In particular, these axisymmetric slab models can provide information on the thermodynamics missing from 3-dimensional models that have so far focussed mostly on wind structure. They may also serve as a component of simplified models of the whole tropical cyclone, most notably as part of the potential intensity theory of Emanuel (1986, 1988, 1995). Another important application is for wind engineering and climate risk applications, as for example in Vickery *et al.* (2000) and references therein. However, we believe that it is important that the limitations and properties of slab models are well understood, precisely because of their usefulness in such applications. The purpose of this paper is to point out some of these limitations.

An important property of depth-averaged models is that the vertical averaging of the nonlinear advection terms inevitably imposes some error, since both the advecting flow and the advected quantity possess strong vertical gradients. This error might be plausibly expected to be more severe in slab models of the TCBL than in other applications, since the large radial gradients and strong inflow in the TCBL implies that the horizontal advection terms are large. Indeed, analysis of 3-dimensional model results shows that these terms play a determining role in the boundary layer dynamics (Kepert 2001; Kepert and Wang 2001; Foster 2008). One purpose of this paper is to quantify the error in these terms due to the depth averaging.

Smith *et al.* (2008) and Smith and Montgomery (2008) have recently compared several depth-averaged models of the TCBL, and shown that some such models make further simplifications in the equations that can have a significant influence on the solutions obtained. The purpose of the research presented here is to extend these

valuable results and further elucidate the characteristics of such models, and to determine and quantify the consequences of the errors imposed by the depth-averaging. The approach will be to compare the results from a fully 3-dimensional model with those from a slab model with the same forcing and physical parameterisations. The three-dimensional model will be that of Kepert and Wang (2001) with the turbulence and surface-flux parameterisations simplified to be more consistent with those typically used in slab models.

2. Model Formulation

a. The depth-averaged model

The equations of motion of a uniform fluid in cylindrical coordinates, suitable for modelling the tropical cyclone boundary layer, are

$$\begin{aligned} \frac{\partial u}{\partial t} + u \frac{\partial u}{\partial r} + \frac{v}{r} \frac{\partial u}{\partial \lambda} + w \frac{\partial u}{\partial z} - \left(f + \frac{v}{r} \right) v \\ = - \left(f + \frac{v_g}{r} \right) v_g + \frac{\partial}{\partial z} \left(K \frac{\partial u}{\partial z} \right), \end{aligned} \quad (1)$$

$$\begin{aligned} \frac{\partial v}{\partial t} + u \frac{\partial v}{\partial r} + \frac{v}{r} \frac{\partial v}{\partial \lambda} + w \frac{\partial v}{\partial z} + \left(f + \frac{v}{r} \right) u \\ = - \frac{1}{\rho r} \frac{\partial p}{\partial \lambda} + \frac{\partial}{\partial z} \left(K \frac{\partial v}{\partial z} \right), \end{aligned} \quad (2)$$

$$\begin{aligned} \frac{\partial \chi}{\partial t} + u \frac{\partial \chi}{\partial r} + \frac{v}{r} \frac{\partial \chi}{\partial \lambda} + w \frac{\partial \chi}{\partial z} \\ = \frac{\partial}{\partial z} \left(K_\chi \frac{\partial \chi}{\partial z} \right) + Q_\chi, \end{aligned} \quad (3)$$

and

$$\frac{\partial r u}{\partial r} + \frac{\partial v}{\partial \lambda} + \frac{\partial r w}{\partial z} = 0, \quad (4)$$

where most symbols have their usual meaning. χ represents any thermodynamic variable and Q_χ represents sources and sinks of the variable, and is included for completeness, although this report will not consider thermodynamic matters. The radial pressure gradient has been written in terms of the gradient wind v_g and is assumed to be constant through the depth of the boundary layer. We shall assume that the turbulent viscosities K and K_χ parameterise all vertical mixing processes, that is, turbulence, rolls

and the effects of shallow convection. Define a vertical averaging operator

$$\bar{\alpha} = \frac{1}{h} \int_0^h \alpha dz \quad (5)$$

where α is any variable and $h = h(r)$ is the boundary layer depth, and let primes denote deviations from this vertical average, $\alpha = \bar{\alpha} + \alpha'$, so that $\overline{\alpha'} = 0$. Then the equations for the vertically averaged wind components are

$$\begin{aligned} \frac{\partial \bar{u}}{\partial t} + \bar{u} \frac{\partial \bar{u}}{\partial r} + \overline{u' \frac{\partial u'}{\partial r}} + \frac{\bar{v}}{r} \frac{\partial \bar{u}}{\partial \lambda} + \frac{\overline{v' \frac{\partial u'}{\partial \lambda}}}{r} + \overline{w \frac{\partial u}{\partial z}} \\ - \left(f + \frac{\bar{v}}{r} \right) \bar{v} - \frac{\overline{v'^2}}{r} \\ = - \left(f + \frac{v_g}{r} \right) v_g + \frac{1}{h} \left[K \frac{\partial u}{\partial z} \right]_{z=0}^{z=h}, \quad (6) \end{aligned}$$

and

$$\begin{aligned} \frac{\partial \bar{v}}{\partial t} + \bar{u} \frac{\partial \bar{v}}{\partial r} + \overline{u' \frac{\partial v'}{\partial r}} + \frac{\bar{v}}{r} \frac{\partial \bar{v}}{\partial \lambda} + \frac{\overline{v' \frac{\partial v'}{\partial \lambda}}}{r} + \overline{w \frac{\partial v}{\partial z}} \\ + \left(f + \frac{\bar{v}}{r} \right) \bar{u} + \frac{\overline{u' v'}}{r} \\ = - \frac{1}{\rho r} \frac{\partial p}{\partial \lambda} + \frac{1}{h} \left[K \frac{\partial v}{\partial z} \right]_{z=0}^{z=h}, \quad (7) \end{aligned}$$

where we have assumed that the pressure gradient force is constant with height. The thermodynamic equation becomes

$$\begin{aligned} \frac{\partial \bar{\chi}}{\partial t} + \bar{u} \frac{\partial \bar{\chi}}{\partial r} + \overline{u' \frac{\partial \chi'}{\partial r}} + \frac{\bar{v}}{r} \frac{\partial \bar{\chi}}{\partial \lambda} + \frac{\overline{v' \frac{\partial \chi'}{\partial \lambda}}}{r} + \overline{w \frac{\partial \chi}{\partial z}} \\ = \frac{1}{h} \left[K_\chi \frac{\partial \chi}{\partial z} \right]_{z=0}^{z=h} + \overline{Q_\chi}, \quad (8) \end{aligned}$$

and the continuity equation is

$$\frac{1}{r} \frac{\partial r \bar{u} h}{\partial r} + \frac{h}{r} \frac{\partial \bar{v}}{\partial \lambda} + w_h = 0, \quad (9)$$

where w_h is the vertical velocity at height h . Note that the perturbation terms do not contribute to w_h , since their vertical integral to height h is 0 by definition. The terms involving vertical derivatives have not been expanded since the vertical derivative of an averaged quantity is not meaningful on its own; the parameterisation of these terms is discussed shortly. Note also that while the algebra leading to these equations is similar

to that in deriving the turbulent flux equations, the averaging operator is different to that used in Reynolds' averaging and the variance and covariance terms here should not be interpreted as turbulent fluxes.

The steady-state axisymmetric equations analysed by Smith (2003); Smith and Vogl (2008); Smith *et al.* (2008); Smith and Montgomery (2008) can be obtained from (6) – (9) by:

1. Neglecting the time derivatives,
2. Neglecting the azimuthal derivatives,
3. Neglecting all the variance and covariance terms,
4. Evaluating the mean vertical advection terms as

$$\overline{w \frac{\partial u}{\partial z}} = -\bar{u} \frac{\min(w_h, 0)}{h}, \quad (10)$$

$$\overline{w \frac{\partial v}{\partial z}} = (v_g - \bar{v}) \frac{\min(w_h, 0)}{h} \quad (11)$$

and

$$\overline{w \frac{\partial \chi}{\partial z}} = (\chi_g - \bar{\chi}) \frac{\min(w_h, 0)}{h}, \quad (12)$$

so that, as discussed by Smith (2003), subsidence into the averaged layer dilutes the properties of the air there with air from above, while ascent simply removes air from the averaged layer without changing the properties of that air that is left behind.

5. Parameterising the turbulent fluxes at the surface

$$\left[K \frac{\partial u}{\partial z} \right]_{z=0} = C_D (\bar{u}^2 + \bar{v}^2)^{1/2} \bar{u}, \quad (13)$$

$$\left[K \frac{\partial v}{\partial z} \right]_{z=0} = C_D (\bar{u}^2 + \bar{v}^2)^{1/2} \bar{v} \quad (14)$$

and

$$\left[K_\chi \frac{\partial \chi}{\partial z} \right]_{z=0} = C_\chi (\bar{u}^2 + \bar{v}^2)^{1/2} (\bar{\chi} - \chi_s). \quad (15)$$

In this report, the drag coefficient C_D and enthalpy transfer coefficient C_χ will be parameterised as in Smith and Montgomery (2008).

6. Parameterising the turbulent fluxes through h as a shallow convection term,

$$\left[K \frac{\partial u}{\partial z} \right]_{z=h} = -w_{sc} \bar{u}, \quad (16)$$

$$\left[K \frac{\partial v}{\partial z} \right]_{z=h} = -w_{sc} (\bar{v} - v_g) \quad (17)$$

and

$$\left[K_X \frac{\partial \chi}{\partial z} \right]_{z=h} = -w_{sc} (\bar{\chi} - \chi_g). \quad (18)$$

Here w_{sc} is a fixed constant velocity scale similar to an entrainment velocity that is set to -0.022 m s^{-1} in Smith (2003), to various values in Smith and Vogl (2008), but zeroed in Smith and Montgomery (2008). This parameter will be set to zero in this paper.

Note that the surface stress is evaluated with the aerodynamic formulae applied to the boundary layer mean wind, rather than to the 10-m wind as would be appropriate for the parameterisations used. The final assumption is that h is imposed as an additional parameter to the model, rather than being calculated as a consequence of the boundary layer dynamics. Usually h is taken to be horizontally uniform, although Smith and Vogl (2008) present some calculations with a radially-varying h .

The preceding paragraph enumerates the assumptions and simplifications made in one group of slab models of the TCBL. Other such models have some differences. For instance, Shapiro (1983) and Vickery *et al.* (2000) retain the azimuthal derivatives, but set both the advective and diffusive fluxes through the top of the boundary layer to 0.

b. The height-resolving model

The model used was described by Kepert and Wang (2001), here with several modifications:

1. The surface layer parameterisation has been replaced by a bulk aerodynamic formulation with the wind-speed dependence of the transfer coefficients of Smith and Vogl (2008).
2. The high-order closure vertical diffusion scheme is replaced by a simple mixing-length scheme, in which the turbulent diffusivity is $K = u_* l$ for a mixing length

$$l = \left((kz)^{-1} + l_\infty^{-1} \right)^{-1} \quad (19)$$

where $l_\infty = 80 \text{ m}$ is the asymptotic mixing length.

3. An option for a slab model is introduced, which solves the time-varying two-dimensional Cartesian coordinate analogue of the equations in Smith and Vogl (2008).

While the model is in Cartesian coordinates, it is run with axisymmetric forcing for this study, and so is effectively a 2-dimensional axisymmetric model. All results were transformed to storm-relative cylindrical coordinates and azimuthally averaged to remove weak spiral band features, for the purposes of this analysis.

3. Results

a. Comparison of bl-mean flow slab and height-resolved models

The flows from the slab and height-resolving models are compared in Fig. 1. This comparison uses the same forcing vortex and surface drag parameterisation in both models; the flow from the height-resolving model is averaged over a similar height range to the prescribed boundary layer depth in the slab model. The slab model has the strongest inflow except within the eye, most markedly so at and immediately outside of the RMW. Thus the eyewall updraft is very much stronger in the slab model. The frictionally-forced updrafts at large radii are more similar, because the $\partial u / \partial r$ term in the continuity equation there compensates for the stronger inflow in the slab model. The height-resolving model has the average azimuthal flow very slightly subgradient except in the vicinity of the RMW, where it is slightly supergradient. This situation is in strong contrast to the slab model, which has much larger departures from gradient balance. Observations show that the azimuthal-mean surface inflow angle in tropical cyclones over the sea is usually in the range $20 - 30^\circ$ (see e.g. Powell 1980). A similar value is obtained here from the height-resolved model. Observations of the height-averaged inflow angle are seldom reported, but we can safely assume it to be less than the surface value. The slab model thus produces an inflow angle that is unrealistically large.

One might suspect that the excess inflow in the slab model is because the

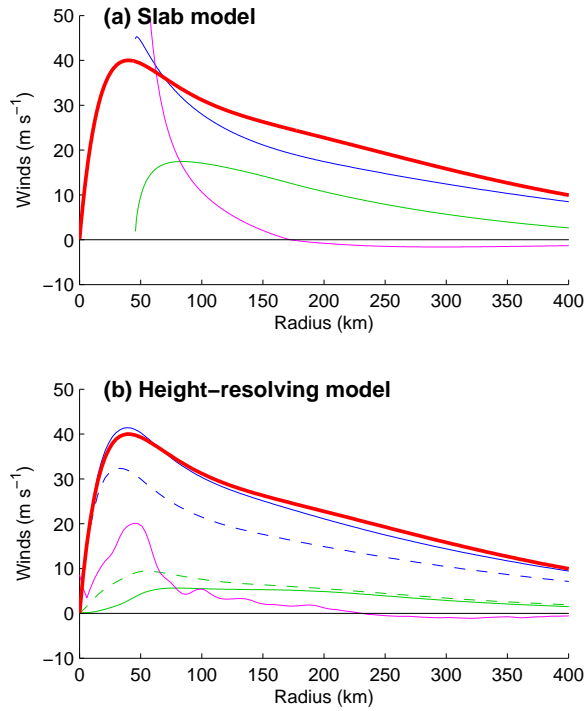


Fig. 1. (a) Axisymmetric boundary layer flow according to the slab model after Smith and co-workers. Gradient wind (thick red), boundary-layer mean azimuthal (blue), inwards (green) and upwards (magenta, multiplied by 100) flow components. Parameter values are as in Smith and Montgomery (2008), including the boundary-layer height which is fixed at $h = 800$ m. (b) Simulation of the same vortex as in (a), except by the height-resolving model. Solid curves are averaged over the lower 850 m except that the vertical velocity is at 850 m. The dashed curves show the flow at 10-m height.

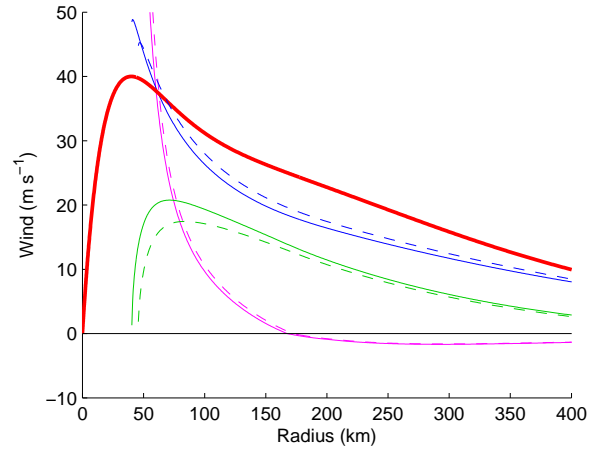


Fig. 2. Axisymmetric boundary layer flow according to the slab model. Gradient wind (thick red), boundary-layer mean azimuthal (blue), inwards (green) and upwards (magenta, multiplied by 100) flow components. Dashed curves are for $f = 5 \times 10^{-5} \text{ s}^{-1}$ and are identical to Fig. 1, solid curves use $f = 3.77 \times 10^{-5} \text{ s}^{-1}$.

surface drag there is calculated from the boundary-layer mean wind, whereas the height-resolving model uses the 10-m wind. One can crudely correct for this by reducing the wind speeds in the surface stress calculation by a factor of, say, 0.8 – 0.9, to better represent the surface wind (see e.g. Kepert and Wang 2001; Franklin *et al.* 2003, and references therein regarding the choice of constant). While this adjustment reduces the departure of the boundary-layer flow from the gradient flow at large radii, this departure is still larger than in the height-resolving model (not shown). In addition, the solution now displays marked oscillations inwards of about twice the RMW similar to those analysed by Smith and Vogl (2008, section 4.1) but beginning at much larger radius (not shown).

b. Further results from axisymmetric slab models

The slab model is unphysically sensitive to the choice of Coriolis parameter. The Rossby number $Ro = v_g/(rf)$ exceeds unity inwards of about 250 km in the simulation in Fig. 1, and is 16 at the RMW. This would normally imply that the Coriolis force should have a diminishing effect on the solution in this region. Instead, comparing the dashed and solid curves in Fig. 2, we see that chang-

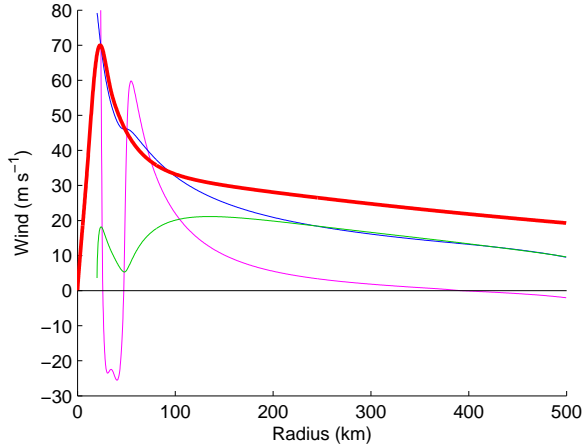


Fig. 3. Simulated axisymmetric flow in the boundary layer of Hurricane Georges on 19 Sept 1998, according to the slab model. Parameter settings are as in Fig 1. Gradient wind (thick red), boundary-layer mean azimuthal (blue), inwards (green) and upwards (magenta, multiplied by 100) flow components. Note the bimodal structure of the inflow and the associated strong downdraft near radius 50 km.

ing f from 5×10^{-5} to $f = 3.77 \times 10^{-5}$, corresponding to 20° and 15° degrees latitude respectively, results in a change of up to 10% in the modelled boundary-layer flow. Such strong sensitivity is strongly at variance with our expectation from scaling arguments. In contrast, the height-resolving model displays almost no sensitivity to the Coriolis parameter (not shown).

The slab model can also produce unphysical results when applied to some vortex profiles. We have tested the slab model on a variety of vortex radial profiles of differing sizes, intensities and structures. An example of especially pathological behaviour is shown in Fig. 3 where the model is forced with the gradient wind radial profile fitted to aircraft and dropsonde observations in Hurricane Georges by Kepert (2006a). The oscillations in \bar{u} and \bar{v} that are apparent inwards of $r = 150$ km seem to have similar dynamics to those analysed near the RMW by Smith (2003) and Smith and Vogl (2008), but have not previously been reported except near and within the RMW. They produce a strong oscillation in the vertical motion, to the extent that the frictionally-forced vertical motion near 50 km, or twice the RMW, is actually downwards. In contrast, the modelled flow from the simulation in

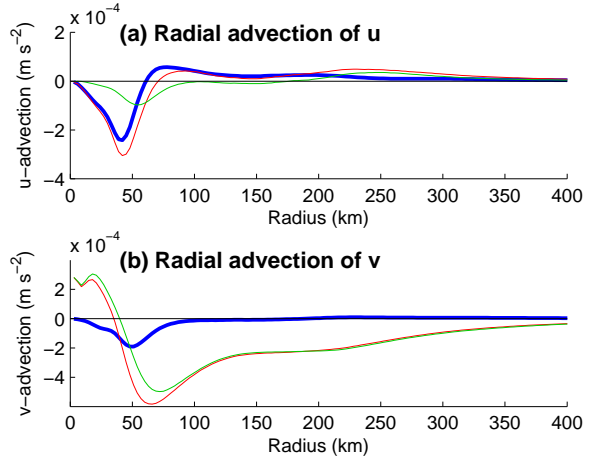


Fig. 4. Radial advection of momentum, averaged to 2-km depth, in the height-resolving simulation shown in Fig. 1b. (a) Radial advection of u . The red curve shows the correct average $-\bar{u}\partial u/\partial r$ and the green the slab-model equivalent, $-\bar{u}\partial \bar{u}/\partial r$. The difference, $-\bar{u}'\partial u'/\partial r$ is shown in blue. (b) As for (a), except for the radial advection of v .

Kepert (2006a), which was shown there to agree well with the observations, does not display this bizarre character.

c. Comparison of momentum budget in slab and height-resolved models

As discussed in section 2a, the depth-averaging of the non-linear terms is inaccurate because of the significant vertical structure in the wind profiles. We may estimate this error using the height-resolving model, although note that this estimate may not capture the full consequences of the error since the slab model is nonlinear. For example, the depth-averaged radial advection of radial wind from the simulation in Fig. 1b is presented in panel (a) of Fig. 4, which shows the true depth-averaged advection $-\bar{u}\partial u/\partial r$ in red, the slab-model equivalent $-\bar{u}\partial \bar{u}/\partial r$ in green, and the difference $-\bar{u}'\partial u'/\partial r$ in blue. It is evident that the difference is substantial, particularly near the RMW. The corresponding calculation for the radial advection of azimuthal wind is shown in panel (b), where the errors are smaller but clearly non-negligible. The other nonlinear terms contain relatively smaller inaccuracies in this case and are not shown.

The slab model equations may be solved by an inwards integration of the equations

for $\partial\bar{u}/\partial r$ and $\partial\bar{v}/\partial r$, where equations for these terms arise from the advection terms in the horizontal momentum equations and therefore contain the inaccuracies analysed in Fig. 4. Such integration implies that any errors, including those noted here, will accumulate. However, all strategies for solving the problem should give the same answer, so the issues noted above with the slab models are a result of the formulation, not the method of solution. In particular, solutions to the problem were obtained using the single-level option of the height-resolving model and were found to be very similar to those obtained from the radial integration, confirming that it is the derivation of the equations and not the method of solution that is the cause of the problems.

4. Improving on Depth-Averaging

a. Formulation

We have seen that the problem with depth-averaged models is that the implicit assumption, that the depth-averaging can be taken inside the nonlinear terms, is poor. Here we present an improved model that assumes a parametric form for the vertical profiles of the model variables. The particular parametric form is chosen to be physically reasonably realistic, and to be amenable to analytical integration of the linear and nonlinear terms. Following some experimentation, and guided by the arguments of Rosenthal (1962), Kepert (2001) and Kepert and Wang (2001), we choose the Ekman spiral in the form

$$u(r, z) = [(u_b(r) - v_b(r)) \cos(z/\delta(r)) + (u_b(r) + v_b(r)) \sin(z/\delta(r))] \exp(-z/\delta(r)) \quad (20)$$

and

$$\tilde{v}(r, z) = [-(u_b(r) - v_b(r)) \sin(z/\delta(r)) + (u_b(r) + v_b(r)) \cos(z/\delta(r))] \exp(-z/\delta(r)) \quad (21)$$

where $v(r, z) = v_g(r) + \tilde{v}(r, z)$, $\delta(r)$ is a prescribed height scale, and u_b and v_b are free parameters that describe the structure of the spiral. Defining a vertical averaging operator

$$\langle \bullet \rangle = \frac{1}{\delta(r)} \int_0^\infty \bullet dz \quad (22)$$

our parametric forms of u and v satisfy

$$\langle u \rangle = u_b \quad (23)$$

$$\langle \tilde{v} \rangle = v_b \quad (24)$$

The parameters u_b and v_b that characterise u and \tilde{v} are thus seen to be the boundary-layer-mean flow perturbation. Also

$$u(r, 0) = u_b(r) - v_b(r) \quad (25)$$

$$v(r, 0) = u_b(r) + v_b(r) + v_g(r) \quad (26)$$

which will be needed for the surface boundary condition. The nonlinear terms are all analytically integrable, in particular

$$\left\langle u \frac{\partial u}{\partial r} \right\rangle = \frac{3u_b^2 - 2u_b v_b + v_b^2}{8\delta} \frac{\partial \delta}{\partial r} + \frac{1}{4} \left(u_b \left(3 \frac{\partial u_b}{\partial r} - \frac{\partial v_b}{\partial r} \right) + v_b \left(-\frac{\partial u_b}{\partial r} + \frac{\partial v_b}{\partial r} \right) \right) \quad (27)$$

$$\left\langle u \frac{\partial \tilde{v}}{\partial r} \right\rangle = \frac{3u_b^2 + 2u_b v_b + v_b^2}{8\delta} \frac{\partial \delta}{\partial r} + \frac{1}{4} \left(u_b \left(\frac{\partial u_b}{\partial r} + 3 \frac{\partial v_b}{\partial r} \right) - v_b \left(\frac{\partial u_b}{\partial r} + \frac{\partial v_b}{\partial r} \right) \right) \quad (28)$$

$$\langle u \tilde{v} \rangle = \frac{1}{4} (u_b^2 + 2u_b v_b - v_b^2) \quad (29)$$

and

$$\langle \tilde{v}^2 \rangle = \frac{1}{4} (u_b^2 + 2u_b v_b + 3v_b^2). \quad (30)$$

These are clearly quite different to the equivalent for a slab model, which would simply be $u_b \partial u_b / \partial r$, and so forth. We demonstrated above that these nonlinear terms are calculated quite inaccurately in the slab model, and the aim here is that imposing a more realistic structure on the vertical profiles will enable us to calculate the averaged nonlinear terms with greater accuracy, and thereby produce a more reasonable model. We may now substitute the parametric u and \tilde{v} (20, 21) into Eqs (1) and (2), omit the time and azimuthal derivatives, apply the vertical averaging operator (22), and rearrange. The diffusion terms become

$$\left\langle \frac{\partial}{\partial z} \left(K \frac{\partial u}{\partial z} \right) \right\rangle = \frac{1}{\delta} \left[K \frac{\partial u}{\partial z} \right]_0^\infty \quad (31)$$

$$\left\langle \frac{\partial}{\partial z} \left(K \frac{\partial \tilde{v}}{\partial z} \right) \right\rangle = \frac{1}{\delta} \left[K \frac{\partial \tilde{v}}{\partial z} \right]_0^\infty \quad (32)$$

and the boundary conditions (13,14) are applied using the surface wind (25, 26), while the upper condition is that the flux approaches zero as $z \rightarrow \infty$. By assuming parametric forms for u and \tilde{v} we are treating the vertical fluxes within the boundary layer due to diffusion and advection implicitly.

The horizontal momentum equations so modified are then rearranged to give a pair of coupled ordinary differential equations

$$\frac{\partial u_b}{\partial r} = f_u(u_b, v_b) \quad (33)$$

$$\frac{\partial v_b}{\partial r} = f_v(u_b, v_b) \quad (34)$$

which can be solved by numerical integration inwards from large radius, similarly to the slab model. The functions f_u and f_v are given in the appendix.

This model is somewhat similar to the momentum integral models of Smith (1968), Leslie and Smith (1970) and Bode and Smith (1975), except that

1. the boundary layer depth scale δ is prescribed, not predicted;
2. the boundary layer perturbations u_b and v_b are additive to v_g , not multiplicative; and
3. a different parametric form is used for the boundary layer perturbations.

We shall see below that it does a nice job of matching the 3-d model results, and seems to avoid some of the undesirable characteristics of the slab model.

There is an inconsistency inherent in this formulation: the chosen profiles imply a stress discontinuity immediately above the surface boundary, since the near-surface shear $\partial/\partial z(u, \tilde{v}) = 2(v_b, -u_b)/\delta$ is generally not in the same direction as the surface wind $(u_b, v_b + v_g)$. This limitation is inherent to the model. We believe that there is unlikely to be a universal choice for parametric profiles which avoids this problem, since the boundary layer structure is sensitive to the storm radial profile of gradient wind (Kepert 2001; Kepert and Wang 2001). Also, we are using two equations, essentially those for the horizontal momentum components, to solve for two unknowns u_b and v_b . The stress continuity condition is a third constraint on the system, which will in general make the system over-determined unless the parametric profiles (20, 21) are re-

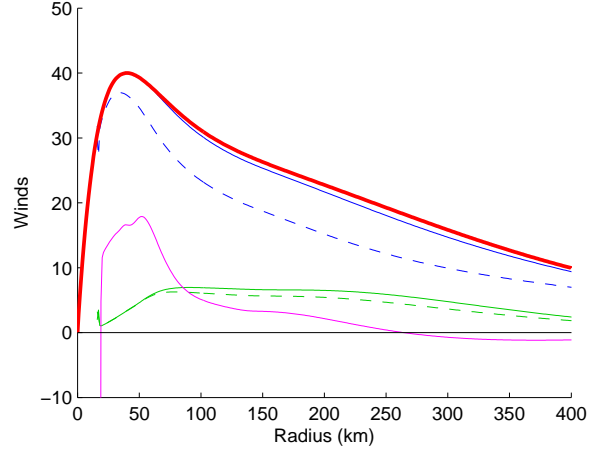


Fig. 5. Axisymmetric boundary layer flow according to the improved model, with constant boundary layer depth of 800 m. Gradient wind (thick red), boundary-layer mean azimuthal (blue), inwards (green) and upwards (magenta, multiplied by 100) flow components. Surface flow shown dashed, same colours.

placed by a form with a third free parameter. Note also that a similar but more severe surface stress inconsistency occurs in slab models, where the surface stress is in the direction of the boundary-layer mean wind. Because of this inconsistency, care should be exercised when using this simplified model, or indeed any simplified model, for quantitative work. Models that are linearised, or depth-averaged, or have the vertical structure parameterised, are useful for elucidating the basic physics only to the extent that the errors introduced are able to be neglected for the level of understanding required.

b. Results with the improved model

Figure 5 shows the predicted flow using the improved model for the same vortex as in Fig. 2. The problems listed in section 3b are all fixed:

1. the boundary-layer-mean azimuthal flow is not strongly different from the gradient flow;
2. the inflow is weaker and the inflow angle is smaller;
3. the updraft near RMW is weaker; and
4. there is barely any sensitivity to f (not shown).

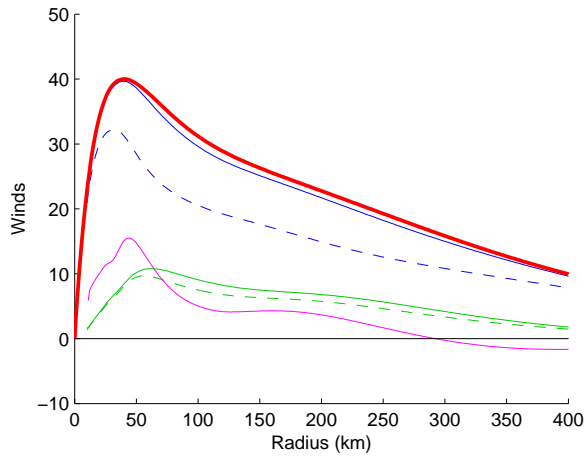


Fig. 6. As in Fig. 5, except for the boundary-layer depth set to 1500 m at radius 500 km and varying with radius as $I^{-1/2}$.

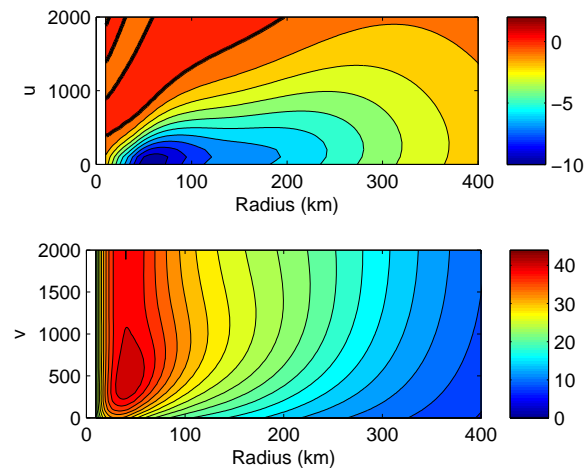


Fig. 7. Axisymmetric boundary layer flow according to the improved model, from the simulation of Fig. 6. Top: radius-height section of radial wind, contour interval 1 m s^{-1} , 0 contour shown bold. Bottom: radius-height section of azimuthal wind, contour interval 2 m s^{-1} .

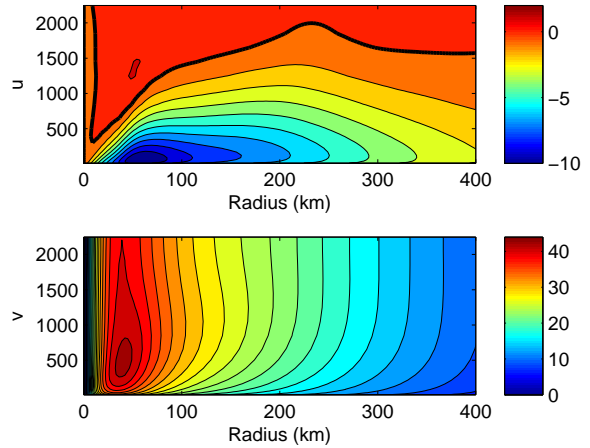


Fig. 8. As in Fig. 7, except according to the height-resolving model.

The improved model also produces physically reasonable results for a wide range of vortex structures.

If the model is run with the boundary layer height varying with radius as $I^{-1/2}$ where I is the inertial stability, in accordance with simple scaling arguments (e.g Eliassen and Lystad 1977; Kepert 2001), then the simulated flow, shown in Fig. 6, resembles that from the height-resolved model even more closely. Further, the radius-height sections in Fig. 7 displays very similar flow to that obtained from the full height-resolved model for the same vortex, shown in Fig. 8.

5. Conclusions

We have demonstrated marked differences in the boundary-layer flow predicted by a simple slab model and that predicted by a height-resolving model. In addition, the slab model was shown to be capable of quite pathological behaviour for some reasonable parameter settings. Analysis of the reasons for these properties is still in progress, but two factors have been shown to contribute:

1. the calculation of the surface drag using the boundary-layer mean wind rather than the surface wind, and
2. the inaccurate treatment of the nonlinear terms in the depth-averaging.

An improved model was presented, which is of similar computational cost to a slab model but was formulated to avoid these problems. Simulations from this model

are much closer to those from the height-resolving model, and the new model is much less prone to producing unphysical results.

Simplified boundary-layer models are useful for a number of purposes, with major applications including climatological risk assessment and engineering design. The inaccuracies demonstrated here must be of significant concern for these applications. A further important application has been as a component of tropical cyclone potential intensity (PI) models. Recently, Smith and Montgomery (2008) have shown that further approximations within a slab model, including those made in Emanuel's PI model, can produce large changes in the flow. Those differences are of similar magnitude to the differences between slab and height-resolved models demonstrated here. Thus, while we agree with Smith and Montgomery (2008) as to the need to improve the important boundary-layer component within existing PI models, we strongly caution that simply relaxing some approximations but remaining with the slab model approach risks replacing one insufficiently accurate model with another. A better solution could be an extension of the improved model presented here, which includes prediction of the thermodynamic parameters also. Research is continuing to develop such a model.

A. The improved model

The full equations for the radial integration of the improved model of section 4 are

$$\begin{aligned}
& 2r(5u_b^2 - 4u_b v_b + v_b^2) \frac{\partial u_b}{\partial r} \\
&= 2u_b^3 + 4u_b^2 v_b + 10u_b v_b^2 - 4v_b^3 \\
&\quad - 4fr(u_b^2 - 4u_b v_b + v_b^2) \\
&\quad - 4v_g(u_b^2 - 7u_b v_b + 2v_b^2) \\
&\quad - 4ru_b \frac{\partial v_g}{\partial r} (u_b - v_b) \\
&\quad - 4rs_0 C_d \delta^{-1} (u_b - v_b)(4u_b + v_g) \\
&\quad - r\delta^{-1} \frac{\partial \delta}{\partial r} (6u_b^3 - 5v_b u_b^2 + 2v_b^2 u_b - v_b^3) \quad (35)
\end{aligned}$$

and

$$\begin{aligned}
& 2r(5u_b^2 - 4u_b v_b + v_b^2) \frac{\partial v_b}{\partial r} \\
&= -4u_b^3 - 6u_b^2 v_b + 4u_b v_b^2 + 2v_b^3 \\
&\quad - 4fr(3u_b^2 - v_b^2) \\
&\quad - 4v_g(3u_b^2 + u_b v_b - 2v_b^2) \\
&\quad - 4ru_b \frac{\partial v_g}{\partial r} (3u_b - v_b) \\
&\quad - 4rs_0 C_d \delta^{-1} \\
&\quad \times (2u_b^2 + 4u_b v_b - 2v_b^2 + (3u_b - v_b)v_g) \\
&\quad - ru_b \delta^{-1} \frac{\partial \delta}{\partial r} (3u_b^2 + 4u_b v_b - v_b^2) \quad (36)
\end{aligned}$$

where s_0 is the surface wind speed,

$$s_0 = ((u_b - v_b)^2 + (u_b + v_b + v_g)^2)^{1/2}. \quad (37)$$

References

- Bell MM, Montgomery MT. 2008. Observed structure, evolution and potential intensity of category five Hurricane Isabel (2003) from 12 – 14 September. *Mon. Wea. Rev.* **136**: 2023 – 2046.
- Bister M, Emanuel KA. 1998. Dissipative heating and hurricane intensity. *Meteorol. Atmos. Phys.* **50**: 233–240.
- Bode L, Smith RK. 1975. A parameterization of the boundary layer of a tropical cyclone. *Boundary Layer Meteor.* **8**: 3–19.
- Deardorff JW. 1972. Numerical investigation of neutral and unstable planetary boundary layers. *J. Atmos. Sci.* **28**: 91–115.
- Eliassen A, Lystad M. 1977. The Ekman layer of a circular vortex. A numerical and theoretical study. *Geophysica Norvegica* **7**: 1–16.
- Emanuel KA. 1986. An air-sea interaction theory for tropical cyclones. Part I: Steady-state maintenance. *J. Atmos. Sci.* **43**: 585–604.
- Emanuel KA. 1988. The maximum intensity of hurricanes. *J. Atmos. Sci.* **45**: 1143–1155.
- Emanuel KA. 1995. Sensitivity of tropical cyclones to surface exchange coefficients and a revised steady-state model incorporating eye dynamics. *J. Atmos. Sci.* **52**: 3969–3976.

- Foster RC. 2008. Boundary layer similarity under an axisymmetric, gradient wind vortex. *draft manuscript xx*: xx.
- Franklin JL, Black ML, Valde K. 2003. GPS dropwindsonde wind profiles in hurricanes and their operational implications. *Wea. and Forecasting* **18**: 32–44.
- Kepert JD. 2001. The dynamics of boundary layer jets within the tropical cyclone core. Part I: Linear theory. *J. Atmos. Sci.* **58**: 2469–2484.
- Kepert JD. 2006a. Observed boundary-layer wind structure and balance in the hurricane core. Part I: Hurricane Georges. *J. Atmos. Sci.* **63**: 2169–2193.
- Kepert JD. 2006b. Observed boundary-layer wind structure and balance in the hurricane core. Part II: Hurricane Mitch. *J. Atmos. Sci.* **63**: 2194–2211.
- Kepert JD, Wang Y. 2001. The dynamics of boundary layer jets within the tropical cyclone core. Part II: Nonlinear enhancement. *J. Atmos. Sci.* **58**: 2485–2501.
- Kuo HL. 1971. Axisymmetric flow in the boundary layer of a maintained vortex. *J. Atmos. Sci.* **28**: 20–41.
- Kuo HL. 1982. Vortex boundary layer under quadratic surface stress. *Boundary-Layer Meteorol.* **22**: 151–169.
- Leslie LM, Smith RK. 1970. The surface boundary layer of a hurricane - part ii. *Tellus* **22**: 288–297.
- Montgomery MT, Snell HD, Yang Z. 2001. Axisymmetric spindown dynamics of hurricane-like vortices. *J. Atmos. Sci.* **58**: 421–435.
- Moss MS, Rosenthal SL. 1975. On the estimation of planetary boundary layer variables in mature hurricanes. *Mon. Wea. Rev.* **103**: 980–988.
- Powell MD. 1980. Evaluation of diagnostic marine boundary-layer models applied to hurricanes. *Mon. Wea. Rev.* **108**: 757–765.
- Powell MD, Houston SH, Reinhold TA. 1996. Hurricane Andrew's landfall in south Florida. Part I: Standardizing measurements for documentation of surface wind fields. *Wea. Forecast.* **11**: 304–328.
- Rosenthal SL. 1962. A theoretical analysis of the field of motion in the hurricane boundary layer. National hurricane research project report no. 56, U. S. Department of Commerce.
- Schwendike J, Kepert JD. 2008. The boundary-layer winds in Hurricanes Danielle (1998) and Isabel (2003). *Mon. Wea. Rev.* **136**: in press.
- Shapiro LJ. 1983. The asymmetric boundary layer flow under a translating hurricane. *J. Atmos. Sci.* **40**: 1984–1998.
- Smith RK. 1968. The surface boundary layer of a hurricane - Part I. *Tellus* **20**: 473–483.
- Smith RK. 2003. A simple model of the hurricane boundary layer. *Quart. J. Roy. Meteor. Soc.* **129**: 1007–1027.
- Smith RK, Montgomery MT. 2008. Balanced boundary layers used in hurricane models. *Quart. J. Roy. Meteor. Soc.* **134**: 1385–1395.
- Smith RK, Montgomery MT, Vogl S. 2008. A critique of Emanuel's hurricane model and potential intensity theory. *Quart. J. Roy. Meteor. Soc.* **134**: 551–561.
- Smith RK, Vogl S. 2008. A simple model of the hurricane boundary layer revisited. *Quart. J. Roy. Meteor. Soc.* **134**: 337–351.
- Vickery PJ, Skerjil PF, Steckley AC, Twisdale L. 2000. Hurricane wind field model for use in hurricane simulations. *J. Engineering Structures* **126**: 1203–1221.